

Robust Swing-Structured Triboelectric Nanogenerator for Efficient Blue Energy Harvesting

Tao Jiang, Hao Pang, Jie An, Pinjing Lu, Yawei Feng, Xi Liang, Wei Zhong, and Zhong Lin Wang*

Ocean wave energy is a promising renewable energy source, but harvesting such irregular, “random,” and mostly ultra-low frequency energies is rather challenging due to technological limitations. Triboelectric nanogenerators (TENGs) provide a potential efficient technology for scavenging ocean wave energy. Here, a robust swing-structured triboelectric nanogenerator (SS-TENG) with high energy conversion efficiency for ultra-low frequency water wave energy harvesting is reported. The swing structure inside the cylindrical TENG greatly elongates its operation time, accompanied with multiplied output frequency. The design of the air gap and flexible dielectric brushes enable minimized frictional resistance and sustainable triboelectric charges, leading to enhanced robustness and durability. The TENG performance is controlled by external triggering conditions, with a long swing time of 88 s and a high energy conversion efficiency, as well as undiminished performance after continuous triggering for 4 00 000 cycles. Furthermore, the SS-TENG is demonstrated to effectively harvest water wave energy. Portable electronic devices are successfully powered for self-powered sensing and environment monitoring. Due to the excellent performance of the distinctive mechanism and structure, the SS-TENG in this work provides a good candidate for harvesting blue energy on a large scale.

1. Introduction

With a rapid development of the world economy, energy has been playing the most critical role. Massive consumption of fossil fuels has brought increasing threats of energy crisis and environmental deterioration,^[1,2] driving people to search for new energy sources urgently from our environment. Ocean waves are one of the most desirable clean and renewable energy sources for large-scope applications, with superior advantages of abundant reserve and little dependence on ambient environment conditions.^[3,4] However, such energy has rarely been exploited due to the lack of effective technology for energy scavenging.^[5,6] Usually ocean waves exhibit at a rather low frequency, so that the dominated technology of electromagnetic generator (EMG) is inapplicable owing to the very low efficiency.^[7,8] Considering that the EMG faces huge challenges of high cost, easily corroded, and low efficiency at low frequency, to develop a cost-effective, light-

weight, and highly efficient technology is of great practical value for water wave energy harvesting.

Triboelectric nanogenerator (TENG, also called as Wang generator) has been invented as a promising technology for converting ambient mechanical energy into electricity, by coupling the triboelectrification^[9,10] and electrostatic induction.^[11] The TENG technology, which adopts an underlying mechanism of Maxwell's displacement current,^[12–14] has been applied to harvest energy from a variety of sources, with unique merits of high power density, high efficiency, and low fabrication cost.^[15–17] Due to its distinct mechanism, the TENG generates higher performance than the EMG at low frequency,^[18] implying a possible killer application for low frequency energy harvesting, such as the mostly ultra-low frequency ocean wave energy. So far, various TENG prototypes have been designed to effectively harvest water wave energy,^[19–32] proving the huge potential toward large-scale blue energy harvesting.^[33,34] However, most of the demonstrated TENG devices have the oscillatory frequency close to the water wave triggering frequency. The very low frequency of water waves induces the TENG to generate low frequency outputs, resulting in low average output performance. The main problem is the lack of the structural design

Prof. T. Jiang, H. Pang, J. An, P. Lu, Y. Feng, X. Liang, W. Zhong,
Prof. Z. L. Wang

CAS Center for Excellence in Nanoscience
Beijing Key Laboratory of Micro-nano Energy and Sensor
Beijing Institute of Nanoenergy and Nanosystems
Chinese Academy of Sciences
Beijing 100083, P. R. China
E-mail: zlwang@gatech.edu

Prof. T. Jiang, H. Pang, P. Lu, Prof. Z. L. Wang
Center on Nanoenergy Research
School of Physical Science and Technology
Guangxi University
Nanning, Guangxi 530004, P. R. China

Prof. T. Jiang, J. An, Y. Feng, X. Liang, W. Zhong, Prof. Z. L. Wang
School of Nanoscience and Technology
University of Chinese Academy of Sciences
Beijing 100049, P. R. China

Prof. Z. L. Wang
School of Materials Science and Engineering
Georgia Institute of Technology
Atlanta, GA 30332-0245, USA

 The ORCID identification number(s) for the author(s) of this article can be found under <https://doi.org/10.1002/aenm.202000064>.

DOI: 10.1002/aenm.202000064

for multiplying the output frequency. Our previous works showed two solutions by introducing a spring structure to store the elastic potential and constructing a pendulum-like structure to realize continuous swing after a mechanical triggering,^[35–37] which can amplify the operation frequency and enhance the energy conversion efficiency. Despite the novel design in the spherical pendulum TENG for high robustness and durability, the output performance needs to be further improved toward practical applications in blue energy, and more explorations on the water wave responses are highly desired to provide an in-depth understanding of the working mechanism.

Herein, we report a robust swing-structured TENG (SS-TENG) with high energy conversion efficiency for harvesting ultra-low frequency water wave energy. An air gap between triboelectric layers and electrodes, and flexible dielectric brushes were designed to decrease frictional resistance and maintain triboelectric charges, thereby enhancing the robustness and durability of TENG. The output characteristics of the SS-TENG were systematically revealed under various mechanical triggering conditions, which focused on the damping output behavior. Then the energy conversion efficiency of the TENG under one triggering and its durability were evaluated. Furthermore, when applied water wave triggering, the performance dependencies of the SS-TENG on the wave frequency and height were detailedly investigated. Finally, the SS-TENG device was applied to successfully power a digital thermometer and a wireless transmitter for self-powered temperature sensing and environment monitoring, demonstrating the extensive applications of TENG toward the blue energy.

2. Results and Discussion

The structure of cylindrical TENG designed with an internal swing structure is schematically shown in Figure 1a. The SS-TENG

consists of a bearing-based swing component supported by two circular acrylic disks through a steel shaft, and a cylindrical acrylic shell whose inner wall is attached by six copper electrodes with equal size and four groups of thin polytetrafluoroethylene (PTFE) stripes. The swing component has three connected-sector acrylic blocks with upper-hollow and lower-solid structure, embedded by three bearings set on the steel shaft. The bottom and top sides of the connected-sector blocks are, respectively, adhered together with an arc-shaped acrylic strip, which is one-twelfth of a cylindrical shell with a central angle of 30°, and several copper blocks are added onto the bottom arc-shaped strip to lower the center of gravity for facilitating the swing motion. The outer surfaces of the arc-shaped acrylic strips having an air gap with the copper electrodes will contact/separate with the PTFE brushes in the swing process. For the six Cu electrodes, all of them have a central angle of nearly 30°, similar to the arc-shaped acrylic strips, and they act as electrodes for four freestanding TENG units connected electrically in parallel. The flexible thin PTFE stripes serve as a charge pump to maintain the triboelectric charges during long time operation, and also the frictional resistance with the acrylic surfaces is very low. In addition, to further decrease the frictional resistance, the connections between the steel shaft and bottom acrylic disks also adopt the anti-friction bearings, and all bearing connections are treated by lubricating oil. Further details of fabrication process can be found in the Experimental Section. The photograph of the as-fabricated SS-TENG device is shown in Figure 1b.

Figure 1c,d shows the schematic working principle of the TENG for the triboelectrification process and electrostatic induction. To enhance the surface charge density, electrons were pre-injected to the PTFE surfaces, leading to negative charges on PTFE before the triboelectrification, as the initial state shown in Figure 1c-i. When an external triggering is

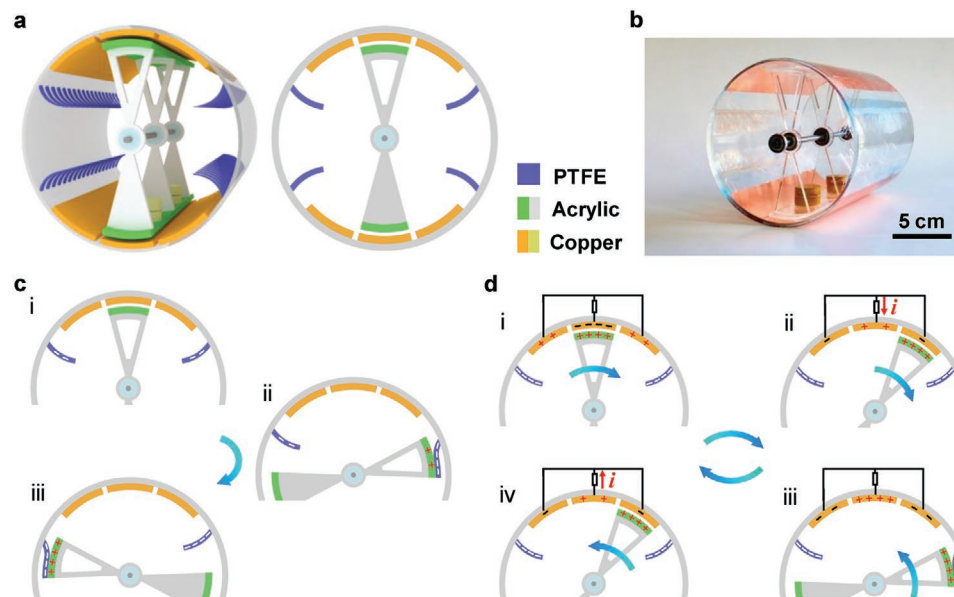


Figure 1. Structure and working principle of the swing-structured TENG. a) Schematic diagram of the 3D structure and cross-section for the swing-structured TENG. b) Photograph of the as-fabricated swing-structured TENG device. c,d) Schematic working principle of the TENG for c) triboelectrification process and d) electrostatic induction, to generate periodic current through the external circuit.

applied to the SS-TENG, i.e., applying an external force onto the cylindrical outside shell, the swing component will naturally swing rightward (or leftward) and contact with the PTFE stripes, generating positive charges on the acrylic surfaces and negative charges on the PTFE surfaces (Figure 1c-ii). Then the swing component moves in a reverse direction to impact the PTFE stripes on the other side for further electrification (Figure 1c-iii). After several cycles, the triboelectric charges on the acrylic and PTFE surfaces get saturated. For simplicity, only half part of the whole TENG is presented. We show the electrification process independently just for better indicating the important role of charging pump of the PTFE stripes from the initial state to the saturated state.

The working of the SS-TENG under an external triggering is based on the electrostatic induction. As shown in Figure 1d, the left and right electrodes are connected, and form the parallel connection of two TENGs together with the shared middle electrode. At the initial state, equal amount of opposite charges is induced on the middle and left/right electrodes, as shown in Figure 1d-i. Under an external triggering, the swing component is driven to swing rightward (Figure 1d-ii), which can easily pass the right electrode until contacting with the PTFE brushes. The swing motion of the positively charged acrylic surfaces causes the free electrons to flow from the middle electrode to the left/right electrodes, generating an induced current across the external circuit. The current flow lasts until the maximum swing amplitude (Figure 1d-iii). Then, the swing component moves backward, and the free electrons will flow back to the middle electrodes from the left/right electrodes, resulting in a reversed current across the load (Figure 1d-iv). If

the swing component moves leftward first under a triggering, the working principle is completely similar. The periodic movement of the swing component under the triggering produces periodic alternative electric output signals. Note that due to the lack of contact between the triboelectric layer and electrodes, and low frictional resistance with the PTFE brushes, the durability of the materials and device can be possibly ensured. In addition, animal furs can also serve as the low friction materials for reducing the material wearing and improving the durability in the operation process of TENG. The TENG device using the animal furs is expected to also have good performance. The detailed material chosen and device performance characterizations for animal fur-based TENG are being carried on and will be reported in the next work.

The basic output characteristics of the SS-TENG device were investigated under the regular triggering of linear motor, as shown in Figure 2. The influence of the maximum acceleration of the motor on the electric outputs was explored, as well as the maximum displacement. The maximum reached speed of the motor was 1 m s^{-1} . Figure 2a–c shows the output voltage, output current, and transferred charge of the SS-TENG with four basic units in parallel connection at various motor accelerations. The motor displacement was fixed as 7 cm. As the motor acceleration increases from 2.5 to 7.5 m s^{-2} , the peak values of voltage and current both increase, but they slightly decrease with further increase of the acceleration, while the peak value of transferred charge gradually increases until reaching the saturated value. Under the currently adopted conditions, the voltage, current, and charge can arrive at 572 V, $6.3 \mu\text{A}$ and 195 nC, respectively, which can be also viewed from the typical results at the

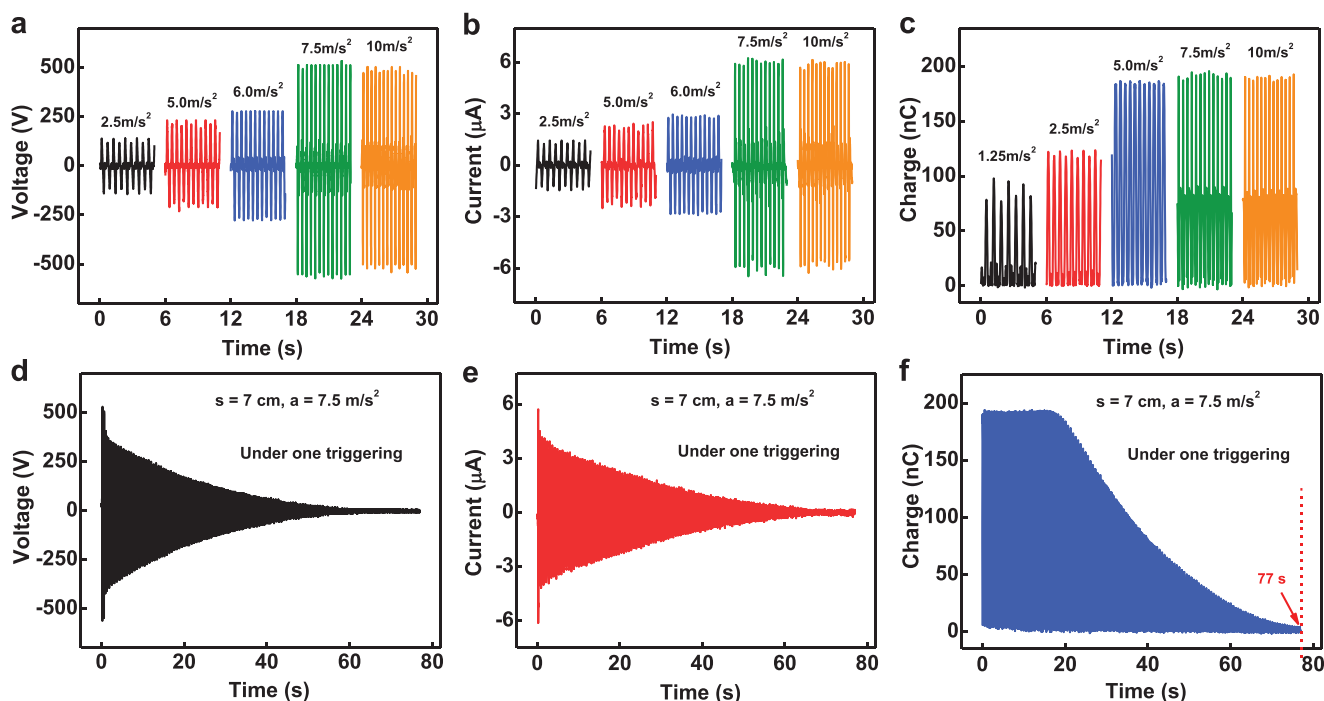


Figure 2. Basic output characteristics of the swing-structured TENG. a–c) Effects of the motor acceleration on a) output voltage, b) output current, and c) transferred charge of the TENG. The maximum displacement and speed of the motor are 7 cm and 1 m s^{-1} , respectively. d) Output voltage, e) output current, and f) transferred charge of the SS-TENG under one triggering. The motor parameters for applying the triggering are $s = 7 \text{ cm}$ and $a = 7.5 \text{ m s}^{-2}$. The swing time is also marked in the profile of transferred charge.

optimum conditions in Figure S1 in the Supporting Information. The drop of the voltage and current at higher motor acceleration is because that the movement of the swing component is hindered by the rapidly moving cylindrical shell. In addition, when we measured the outputs for the bottom half of the SS-TENG, similar effect of the motor acceleration was discovered, but only half of the peak values for the output signals were achieved (Figure S2, Supporting Information).

The damping output behavior of the SS-TENG under one external triggering was illustrated in Figure 2d-f. As can be seen, after the triggering, the amplitudes of the output voltage and current gradually decay until zero with the damped oscillation of the swing component arising from the air resistance. However, the amplitude of the transferred charge first maintains at the maximum value and then decreases with the swing motion. The initial plateau of the charge profile is because the swing amplitude is beyond all the Cu electrodes. The swing motion can last for 77 s at the triggering conditions of 7 cm and 7.5 m s⁻². The swing frequency can be obtained to be about 1.62 Hz from the period/frequency of the charge signals at the time of 10 and 40 s (Figure S3, Supporting Information).

A classic vibratory analysis was done to determine the dynamics of the oscillation system. First, we used the linear motor to apply a periodic triggering to force the device into a vibratory motion for obtaining the relationship between the swing amplitude and external triggering frequency. The motor displacement and maximum velocity were set as 10 cm and 1 m s⁻¹, with no pause during the motion process, and adjusting the motor acceleration can correspond to different triggering frequencies. The detailed results can be found in Figure S4a and Note S1 in the Supporting Information. The swing angle amplitude can get the maximum value at about 1.6 Hz, implying that the resonant frequency of the device is about 1.6 Hz, which is consistent with the output frequency of the TENG and close to the theoretically calculated intrinsic frequency (1.88 Hz). Also, the electric outputs of the device at different frequencies were measured, indicating that the highest outputs of the TENG device were exhibited at the frequency of 1.6 Hz, as shown in Figure S5 in the Supporting Information. Furthermore, the swing angle amplitude and system potential energy with the cycle number during the swing process after one triggering were evaluated (Figure S4b,c and Note S1, Supporting Information). An average quality factor of 112.27 implies that the oscillation system of our SS-TENG is weakly damped.

Besides, the influence of the motor displacement on the electric outputs was also addressed, as shown in Figures S6 and S7 in the Supporting Information. At a higher motor acceleration (7.5 m s⁻²), the peak values of output voltage, output current, and transferred charge all increase with increasing the maximum displacement of the motor (Figure S6, Supporting Information), which is contributed to the increase in the swing amplitude. However, at a lower motor acceleration (5.0 m s⁻²), the peak voltage, current, and charge all have higher values at smaller displacement such as 1 cm, and then decrease to the minimum value, followed by a slight increase (Figure S7a-c, Supporting Information). The different influence of motor displacement on the output performance at a lower acceleration is attributed to the matching between the external triggering frequency and device intrinsic frequency. Interestingly, the swing

time for the TENG can reach 88 s under the triggering conditions of 1 cm and 5 m s⁻² (Figure S7d, Supporting Information), where the demonstration of lighting up light-emitting diodes (LEDs) by the cylindrical SS-TENG is also shown in Video S1 in the Supporting Information.

The SS-TENG is very desirable for harvesting the energy from ultra-low frequency motions due to the continuous swing after the external triggering. Figure 3a,b and Figure S8a in the Supporting Information present the output voltage, transferred charge, and output current profiles of the SS-TENG when applied a triggering every 60 s. The triggering conditions for the linear motor were still 7 cm and 7.5 m s⁻², while the time interval between adjacent excitations was set to ensure the triggering period of 60 s. The electric outputs all have a gradual decaying process, and can last during the 60 s with the output frequency of 1.62 Hz, producing about 100 output cycles under one triggering. The external triggering frequency is 0.017 Hz, which has been multiplied by 95 times due to the swing structure. Figure 3c shows the resistive output behaviors, including the peak output power, average output power-resistance relationships under continuous triggering at 7 cm and 7.5 m s⁻², and translated energy-resistance relationship under one triggering. The average power can be obtained by the harvested energy per unit time, and the harvested energy during one triggering can be calculated by the following equation

$$E_{\text{out}} = \int I(t)^2 R dt \quad (1)$$

where the $I(t)$ is the current across the resistor at the time t , and R is the resistance. It can be found that under such conditions, the TENG can deliver the maximum peak power of 4.56 mW at a matched resistance of 300 MΩ, maximum average power of 0.48 mW at 300 MΩ, and the maximum energy of 11.44 mJ at 500 MΩ. According to the device volume, the peak power density and average power density are obtained to be 1.29 and 0.14 W m⁻³, respectively.

The output performance of our SS-TENG was also compared with other TENG designs previously reported, mainly focusing on the ball-shell structured TENG (BS-TENG) and spherical pendulum TENG (SP-TENG). The peak power density and translated energy density under one triggering for the three TENG designs are listed in Table S1 in the Supporting Information for clear comparison. It is apparent that the peak power density and the translated energy density of SS-TENG are both much larger than those of the SP-TENG, although it has the similar pendulum structure. The improvement of output performance is of great significance toward practical self-powered applications. When comparing with the BS-TENG, our SS-TENG has a lower peak power density, but a higher energy density under one triggering. It implies that our SS-TENG can generate higher energy per unit volume at an ultra-low frequency than the BS-TENG. Therefore, our SS-TENG is more suitable for harvesting the ultra-low frequency energy, such as the water wave energy.

Subsequently, we evaluated the energy conversion efficiency of the SS-TENG under one triggering. The energy conversion process can be divided into two processes: the conversion from input energy by the external impact force to the internal oscillatory energy of the swing component in the TENG device, and

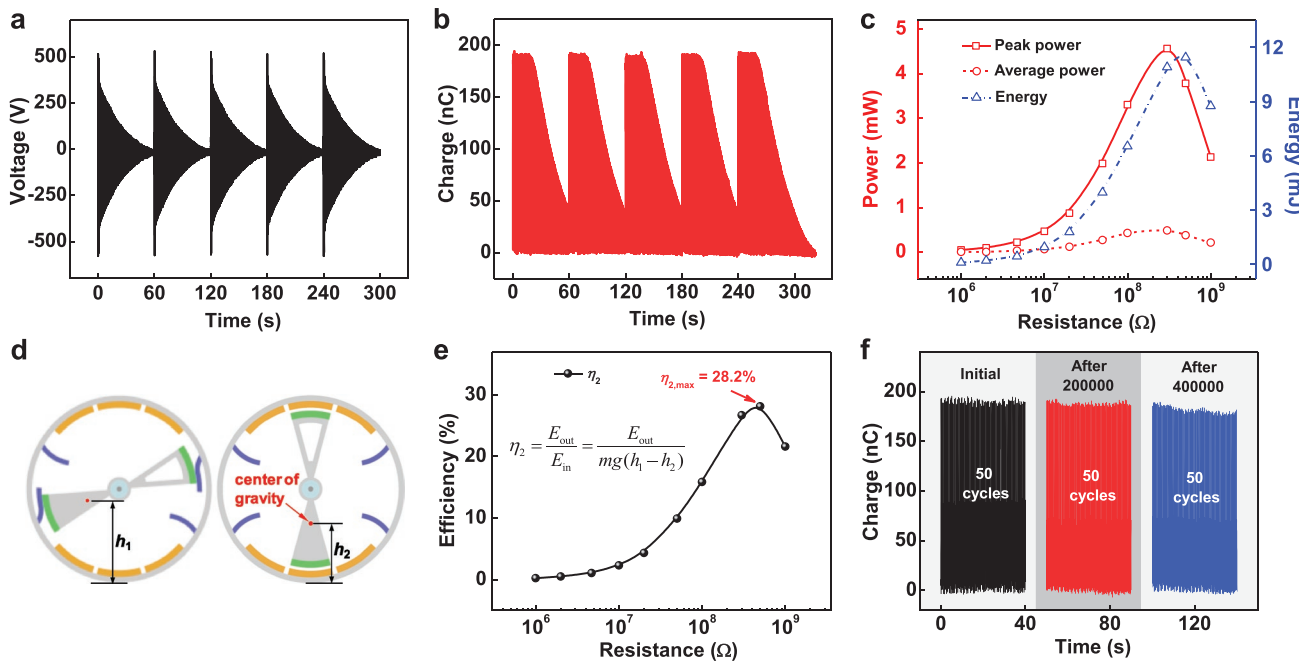


Figure 3. Output performance at ultra-low frequency triggering and durability of the SS-TENG. a) Output voltage and b) transferred charge of the TENG by applying an external triggering every 60 s. c) Peak output power, average output power-resistance relationships under continuous triggering at $s = 7\text{ cm}$ and $a = 7.5\text{ m s}^{-2}$ and translated energy-resistance relationship under one triggering. d) Schematic diagram for the calculation method of energy conversion efficiency η_2 . The state at the highest center of gravity and the final state after the triggering are shown. e) Energy conversion efficiency η_2 with respect to the load resistance. f) Durability result for the transferred charge of the TENG at various cycles.

the oscillatory energy-to-electric energy conversion. The efficiency in the first conversion process was defined as the ratio of acquired oscillatory energy to the input energy of linear motor, while the efficiency in the second process was calculated through the output electric energy after the triggering divided by the acquired mechanical energy. The mechanical energy acquired can be reflected by the difference between the gravitational potential energy at the highest center of gravity and that at the final state after one triggering, as schematically shown in Figure 3d. Therefore, the efficiency in the second process is given by

$$\eta_2 = \frac{E_{\text{out}}}{E_{\text{in}}} = \frac{\int I(t)^2 R dt}{mg(h_1 - h_2)} \quad (2)$$

where m is the mass of the swing component, g is the gravitational acceleration, and h_1 , h_2 are the heights between the center of gravity and the cylinder shell bottom for the two states in Figure 3d. We obtained the values of the heights h_1 and h_2 by extracting the photographs for the two states (Figure S8b, Supporting Information) from a slow motion video of the TENG movement (Video S2, Supporting Information). The detailed calculation method for the energy conversion efficiency can be found in Note S2 of the Supporting Information. We calculated the efficiency η_2 for the TENG at various load resistances and found that the maximum efficiency can reach 28.2% achieved at the matched resistance of $500\text{ M}\Omega$ (Figure 3e). The efficiency, which is an average value, is lower than other type TENG such as the liquid metal-based TENG,^[16] which is mainly dominated by the noncontacting structure design. The air gap

existing between the acrylic surfaces and electrodes decreases the output energy, although it can avoid the material wearing. The efficiency in the first conversion process was obtained through estimating the input energy provided by the linear motor, so the total energy conversion efficiency could be calculated (Note S2, Supporting Information). In addition, based on this swing structure design, we fabricated the smallest device with a length of 10 cm and a diameter of 8 cm. The decrease in the device size will hinder the motion of the swing component, leading to shorter swing time, smaller translated energy, and eventually lower energy conversion efficiency.

Besides the efficiency for the SS-TENG, the durability tests were carried out for 4 00 000 cycles under the triggering conditions of 7 cm and 7.5 m s^{-2} . The transferred charge of the TENG at various cycles is shown in Figure 3f. It can be seen that the transferred charge nearly keeps unchanged after the triggering of 4 00 000 cycles, verifying the excellent durability of the SS-TENG. The super durability is mainly attributed to the design of flexible PTFE brushes, which can maintain the triboelectric charges for long time, and also the little frictional resistance arising from the noncontacting electrostatic induction. Compared with other TENG designs for water wave applications, these advantages of amplifying the output frequency, high mechanical-to-electric energy conversion efficiency, and excellent durability make the SS-TENG act as a superior candidate for harvesting ultra-low frequency energy.

Furthermore, the frequency responses of the output and charging performance of the SS-TENG at lower frequencies were investigated to reveal the device superiority, as shown in Figure S9 in the Supporting Information. The output voltage,

output current, and transferred charge of the SS-TENG at various triggering frequencies are shown in Figure S9a–c in the Supporting Information. The various frequencies were realized through adjusting the time interval of applying adjacent excitations, such as a time interval of 60 s for 0.017 Hz and a time interval of 10 s for 0.1 Hz. It can be found that with increasing the frequency, the amplitudes of the voltage, current, charge all have no great changes, but the output profiles show different damping behavior. The output voltage and current can no longer decay at the frequency of 0.5 Hz, while the charge does not decay at 0.05 Hz. The SS-TENG exhibits excellent energy harvesting ability at the ultra-low or low frequencies. Figure S9d in the Supporting Information shows the charging voltage on a capacitor of 10 μ F for the SS-TENG working at various frequencies. At a lower frequency, the charging voltage is relatively low, but when the frequency reaches 0.05 Hz, the charging profiles will overlap without difference in charging performance due to the swing feature of TENG. The charging performance of the SS-TENG to different capacitors at 0.05 Hz in Figure S9e in the Supporting Information further validates its good energy harvesting ability at ultra-low frequency.

The output performance of the SS-TENG device under the real water wave triggering was measured in a standard water tank through a water wave generator to obtain controllable water waves. Similar to our previous work,^[38] the frequency and height of the water waves can be controlled by the dwell time and crank length. The detailed measurement method can be found in the Experimental Section. Figure 4a–d and Figure S10a,b in the Supporting Information show the influences of the water wave frequency and wave height on the

output voltage, current, and transferred charge for the sealed cylindrical SS-TENG device. With increasing the water wave frequency at a fixed wave height of 10 cm, the voltage, current, and charge all first increase and then decrease, exhibiting an optimum frequency of 1.2 Hz for producing the highest outputs. The optimum frequency is not equivalent to that under the regular triggering, which is ascribed to the complex solid–fluid interaction. Since the actual working condition of the TENG is in the water waves, the experiments in the tank are more practical. On the other hand, the voltage, current, and charge all increase with the wave height, due to the increased impact force of water waves, although the changes are not obvious. The SS-TENG can produce the maximum outputs 342 V, 5.9 μ A, and 256 nC under the water wave triggering. Note that the transferred charge generated in the water waves is larger than that on the linear motor, implying that the device can have greater motion amplitude in the water waves due to the multidirectional impact of water waves to the outside shell.

The resistance dependence of the output performance for the SS-TENG was also characterized, as shown in Figure 4e,f and Figure S10c in the Supporting Information. Under the optimum wave conditions of 10 cm and 1.2 Hz, the peak power, average power, and translated energy of the SS-TENG can be calculated to be 0.51 mW (power density of 144.3 mW m^{-3}), 0.093 mW (power density of 26.3 mW m^{-3}), and 2.17 mJ. The corresponding matched load resistances are, respectively, 20, 50, and 50 M Ω , which are lower than those under the linear motor triggering. That is because the capacitance increases due to the dielectric shielding effect of water. To realize better complete water waves for facilitating the measurements, we generated

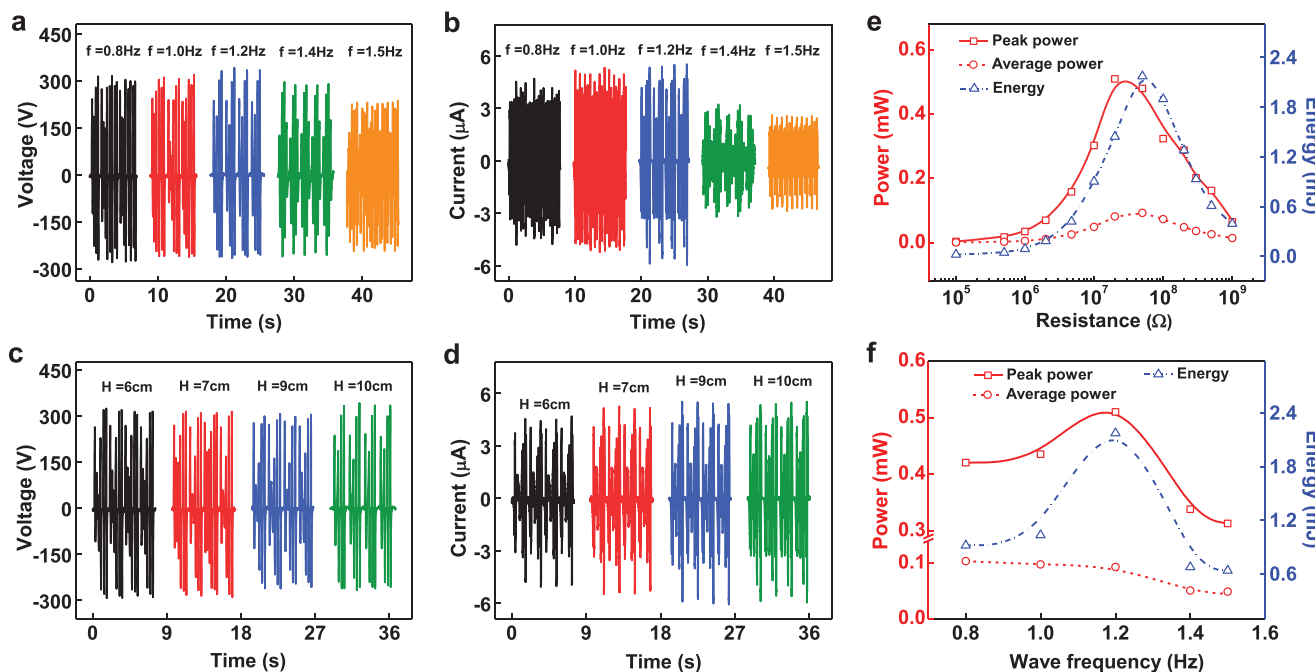


Figure 4. Output performance of the SS-TENG under water wave triggering. a,b) Influence of the water wave frequency on the a) output voltage and b) output current of the sealed cylindrical SS-TENG device. The water wave height was chosen as 10 cm. c,d) Influence of the water wave height on the c) output voltage and d) output current of the TENG device. The water wave frequency was chosen as 1.2 Hz. e) Peak power, average power, and translated energy as functions of the load resistance for the SS-TENG under the wave conditions of 10 cm and 1.2 Hz. f) Influence of the wave frequency on the maximum values of peak power, average power, and energy of the TENG at fixed wave height of 10 cm.

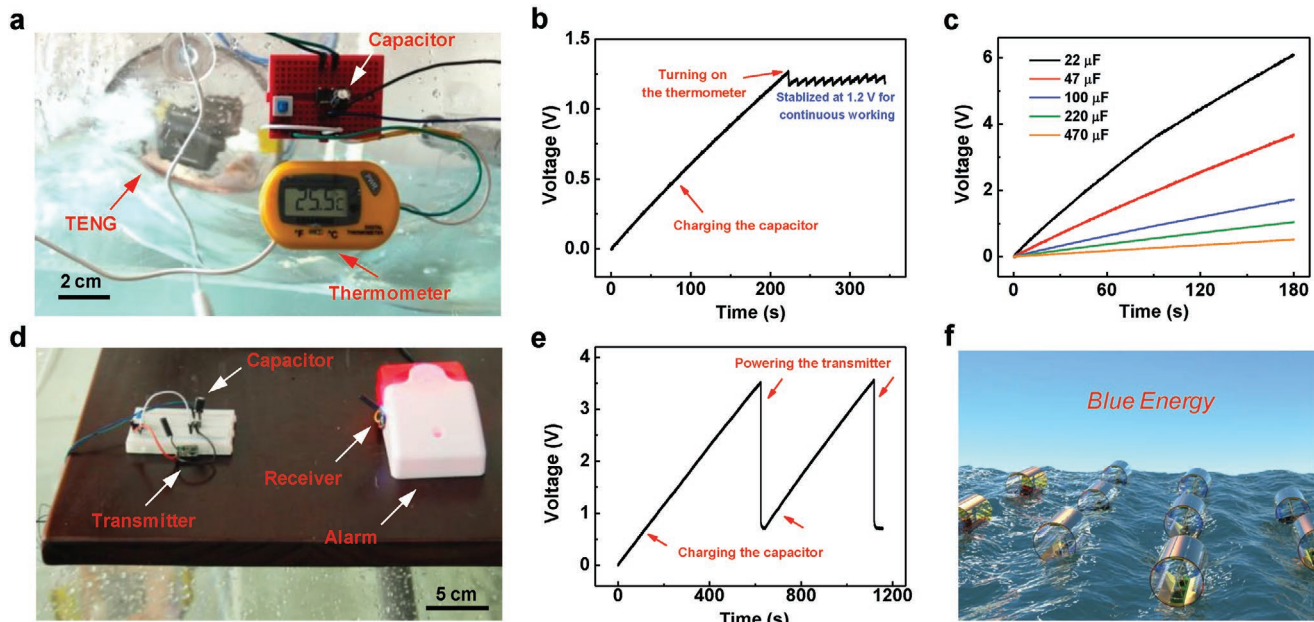


Figure 5. Application demonstrations of the SS-TENG for blue energy harvesting. a) Photograph of a digital thermometer powered by the SS-TENG device under the water wave triggering. b) Charging and discharging process for a capacitor of $220\text{ }\mu\text{F}$ to power the thermometer under the wave conditions of 10 cm and 1.2 Hz. c) Charging voltage on various capacitances for the TENG. d) Photograph of a wireless transmitter powered by the water wave-driven SS-TENG through charging a capacitor of $220\text{ }\mu\text{F}$, which sends a signal to the receiver to turn on the alarm. e) Charging and discharging process for a capacitor of $220\text{ }\mu\text{F}$ to power the transmitter for two consequent transmitting cycles. f) Proposed TENG network by integrating a large number of cylindrical SS-TENG units for large-scale blue energy.

two cycles of water waves instead of one cycle between two pauses. The translated energy after the triggering of two waves was also calculated through Equation (1). The typical output profiles after the triggering of two waves can be seen in Figure S11 in the Supporting Information. Note that at the optimum wave conditions, the total wave energy-to-electric energy conversion efficiency was evaluated (Note S3, Supporting Information). Although the current efficiency is not high enough, considering the abundant reserves of ocean wave energy, our TENG could provide a promising strategy to convert the water wave energy.

Figure 4f shows the effects of the water wave frequency on the peak power, average power, and energy, indicating the optimum frequency characteristic for the output power and energy. And at a fixed wave frequency of 1.2 Hz, the power and energy were found to increase with increasing the wave height (Figure S10c, Supporting Information). For showing the capacity of the SS-TENG for harvesting ultra-low frequency water wave energy, we generated the water waves at a certain time interval to obtain the various low frequencies (0.05–0.4 Hz). The output results with the damping feature are shown in Figure S12 in the Supporting Information. When the frequency arrives at 0.2 Hz, the decaying behavior becomes not obvious, with a continuous charge. At the low frequency, there also exists the optimum frequency of 0.2 Hz to generate the highest average power (Figure S12d, Supporting Information).

Subsequently, the applications of powering portable electronic devices for the SS-TENG through harvesting water wave energy were demonstrated. We chose LEDs, a digital thermometer, and a wireless transmitter for examples. The water wave conditions with the frequency of 1.2 Hz and height of 10 cm

were mainly adopted. The SS-TENG was placed into a sealed square acrylic box to increase the air gap between the electrodes and water surface to diminish the dielectric shielding of water. Under such packaging, the output current and transferred charge both slightly decrease, but the profiles become relatively more regular and stable (Figure S13a,b, Supporting Information). After the water waves stop, the swing characteristic of the SS-TENG makes it continue to light up scores of LEDs as shown in Video S3 in the Supporting Information.

Figure 5a shows the photograph of a digital thermometer powered by the SS-TENG device under the water wave triggering of 1.2 Hz and 10 cm to detect the water temperature through charging a capacitor of $220\text{ }\mu\text{F}$. The charging and discharging process for the capacitor to power the thermometer is shown in Figure 5b. After the capacitor was charged to 1.25 V, the thermometer was connected to the circuit, and turned on to measure the water temperature. The charging voltage can maintain stable at about 1.2 V, and the thermometer can continuously work and display the water temperature, implying that the harvested energy by the SS-TENG device is approximately equivalent to the consumption of the thermometer. For demonstrating the capacity of the SS-TENG in harvesting low-frequency wave energy, a video for powering the digital thermometer at the frequency of 0.2 Hz (applying two waves per 10 s) is shown in Video S4 in the Supporting Information. After the thermometer was turned on, it also could constantly work. Then the capabilities of the TENG for charging different capacitors were also investigated, as presented in Figure 5c. The voltage of the capacitor of $470\text{ }\mu\text{F}$ can be raised to 0.526 V within 180 s by the SS-TENG device under the water waves,

corresponding to an output charge of 247 μ C. The charging performance of the TENG under the lower frequency wave triggering was also measured, indicating that the voltage on the 220 μ F capacitor can arrive at 0.5 V within 81–124 s for the frequency range of 0.05–0.8 Hz (Figure S13c, Supporting Information).

Besides the digital thermometer, the application of driving a wireless transmitter to send a signal to the receiver to turn on the alarm, for self-powering environment monitoring, is also shown in Figure 5d,e and Video S5 in the Supporting Information. The wireless transmitter can send signals to the receiver at a long distance of above 10 m, but due to the space limitation, we only show the case when they are placed together. After the capacitor of 220 μ F was charged from 0 V to about 3.5 V in 623 s, the switch was closed, and the transmitter was powered up to send a signal to the receiver, which turned on the alarm to send out sound and light. The voltage variation of the capacitor for two consequent transmitting cycles is shown in Figure 5e. After the first cycle, the charging time for sending signals is about 475 s. Powering the digital thermometer and transmitter successfully has demonstrated the potential application of the SS-TENG in large-scale blue energy harvesting, which will be realized by connecting a large number of TENG units into a network, as schematically shown in Figure 5f.

3. Conclusion

In summary, we have designed and fabricated a robust SS-TENG with high energy conversion efficiency for harvesting ultra-low frequency water wave energy. The flexible dielectric brushes can ensure replenished charges for electrostatic induction, and the air gap between the electrodes and triboelectric layers realizes little frictional resistance for strong robustness and durability. The influences of external regular triggering conditions on the output performance of the SS-TENG were investigated, showing the maximum peak power of 4.56 mW and an average power of 0.48 mW under the motor parameters of 7 cm and 7.5 m s^{-2} . Importantly, the device can realize the longest swing time of 88 s under one triggering, and exhibits excellent durability. Also, the SS-TENG exhibits excellent capacity for harvesting ultra-low frequency energy. Furthermore, the SS-TENG was applied to harvest the water wave energy, and its performance was found to be controlled by the water wave frequencies and wave heights. Finally, portable electronics were successfully powered by the SS-TENG under the water waves, demonstrating the applications in self-powered temperature sensing and environment monitoring for blue energy.

4. Experimental Section

Fabrication of the SS-TENG Device: First, the swing component was fabricated using a steel shaft with a diameter of 6 mm to support the commercial bearings with an inner diameter of 6 mm and an outer diameter of 17 mm. Three connected-sector acrylic blocks with a circular hole of 17 mm, embedded with a bearing, were fabricated by the laser cutting machine. The hollow and solid sides of the connected-sector blocks were, respectively, adhered together with an arc-shaped acrylic strip, which was obtained by dividing a cylindrical shell (length: 18 cm,

outer diameter: 14 cm, thickness: 2.5 mm) into 12 equal pieces. Second, the cylindrical shell with a length of 20 cm, a thickness of 3 mm, and an outer diameter of 15 cm was prepared as the substrate for electrodes and PTFE stripes, forming a gap of about 1.5 mm between the triboelectric acrylic surfaces and electrodes. Six Cu electrodes with the same central angle as the arc-shaped acrylic strips were adhered onto the internal wall of the cylindrical shell. Electrons were pre-injected to the surfaces of 50 μ m thick PTFE film by the corona discharging method through placing the PTFE film onto the bottom copper surface at a polarization voltage of 5 kV for 6 min, and then thin PTFE stripes were obtained by cutting. Third, the swing component and cylindrical shell were assembled together through two bearings embedded into the two bottom acrylic disks, and the four basic TENG units were connected electrically in parallel. Finally, the cylindrical TENG was sealed and waterproofed by the tile cement for working in the water environment. When charging the capacitors, a square acrylic box was also fabricated to accommodate the cylindrical TENG to decrease the dielectric shielding effect.

Electric Measurements of the TENG Device: The electric output signals of the SS-TENG device were measured under the ideal triggering generated by a linear motor or under the real water wave triggering. The water waves were generated by combing a wave generating mechanism and rebound wave absorber, similar to the previous work.^[38] A programmable digital controller was applied to control the crank rotation to induce the swing of push plate, where the frequency and height of water waves could be adjusted by varying the dwell time and crank length. The output current and transferred charge of the TENG devices, and charging voltage on capacitors were measured by a current preamplifier (Keithley 6514 System Electrometer), while the output voltage of the TENG devices under the ideal triggering and water wave triggering was measured by a digital oscilloscope (Agilent InfiniiVision 2000X).

Supporting Information

Supporting Information is available from the Wiley Online Library or from the author.

Acknowledgements

T.J., H.P., and J.A. contributed equally to this work. Support from the National Key R & D Project from Minister of Science and Technology (2016YFA0202704), National Natural Science Foundation of China (grant nos. 51432005, 51702018, and 51561145021), and Youth Innovation Promotion Association, CAS, are appreciated. The authors also thank Jinhui Nie, Yu Bai, and Pengfei Chen for device fabrications and measurements.

Conflict of Interest

The authors declare no conflict of interest.

Keywords

blue energy, enhanced robustness/durability, swing structured TENGs, triboelectric nanogenerators, wave energy harvesting

Received: January 7, 2020

Revised: March 20, 2020

Published online:

[1] J. P. Painuly, *Renewable Energy* **2001**, *24*, 73.

[2] A. Khaligh, O. C. Onar, *Energy Harvesting: Solar, Wind, and Ocean Energy Conversion Systems*, CRC Press, Boca Raton, FL **2009**.

- [3] A. F. deO. Falcao, *Renewable Sustainable Energy Rev.* **2010**, *14*, 899.
- [4] Z. L. Wang, J. Chen, L. Lin, *Energy Environ. Sci.* **2015**, *8*, 2250.
- [5] S. H. Salter, *Nature* **1974**, *249*, 720.
- [6] J. Falnes, *Mar. Struct.* **2007**, *20*, 185.
- [7] A. V. Jouanne, *Mech. Eng.* **2006**, *128*, 24.
- [8] R. Henderson, *Renewable Energy* **2006**, *31*, 271.
- [9] X. Ma, S. Li, S. Dong, J. Nie, M. Iwamoto, S. Lin, L. Zheng, X. Chen, *Nano Energy* **2019**, *66*, 104090.
- [10] S. Li, Y. Fan, H. Chen, J. Nie, Y. Liang, X. Tao, J. Zhang, X. Chen, E. Fu, Z. L. Wang, *Energy Environ. Sci.* **2020**, *13*, 896.
- [11] F. R. Fan, Z. Q. Tian, Z. L. Wang, *Nano Energy* **2012**, *1*, 328.
- [12] Z. L. Wang, *Mater. Today* **2017**, *20*, 74.
- [13] Z. L. Wang, T. Jiang, L. Xu, *Nano Energy* **2017**, *39*, 9.
- [14] Z. L. Wang, *Nano Energy* **2020**, *68*, 104272.
- [15] G. Zhu, Y. S. Zhou, P. Bai, X. S. Meng, Q. S. Jing, J. Chen, Z. L. Wang, *Adv. Mater.* **2014**, *26*, 3788.
- [16] W. Tang, T. Jiang, F. R. Fan, A. F. Yu, C. Zhang, X. Cao, Z. L. Wang, *Adv. Funct. Mater.* **2015**, *25*, 3718.
- [17] J. Nie, Z. Wang, Z. Ren, S. Li, X. Chen, Z. L. Wang, *Nat. Commun.* **2019**, *10*, 2264.
- [18] Y. Zi, H. Guo, Z. Wen, M.-H. Yeh, C. Hu, Z. L. Wang, *ACS Nano* **2016**, *10*, 4797.
- [19] X. F. Wang, S. M. Niu, Y. J. Yin, F. Yi, Z. You, Z. L. Wang, *Adv. Energy Mater.* **2015**, *5*, 1501467.
- [20] T. Jiang, L. M. Zhang, X. Y. Chen, C. B. Han, W. Tang, C. Zhang, L. Xu, Z. L. Wang, *ACS Nano* **2015**, *9*, 12562.
- [21] L. Xu, T. Jiang, P. Lin, J. J. Shao, C. He, W. Zhong, X. Y. Chen, Z. L. Wang, *ACS Nano* **2018**, *12*, 1849.
- [22] P. Cheng, H. Guo, Z. Wen, C. Zhang, X. Yin, X. Li, D. Liu, W. Song, X. Sun, J. Wang, Z. L. Wang, *Nano Energy* **2019**, *57*, 432.
- [23] T. X. Xiao, X. Liang, T. Jiang, L. Xu, J. J. Shao, J. H. Nie, Y. Bai, W. Zhong, Z. L. Wang, *Adv. Funct. Mater.* **2018**, *28*, 1802634.
- [24] X. Liang, T. Jiang, G. Liu, T. Xiao, L. Xu, W. Li, F. Xi, C. Zhang, Z. L. Wang, *Adv. Funct. Mater.* **2019**, *29*, 1807241.
- [25] X. Liang, T. Jiang, G. Liu, Y. Feng, C. Zhang, Z. L. Wang, *Energy Environ. Sci.* **2020**, *13*, 277.
- [26] T. X. Xiao, T. Jiang, J. X. Zhu, X. Liang, L. Xu, J. J. Shao, C. L. Zhang, J. Wang, Z. L. Wang, *ACS Appl. Mater. Interfaces* **2018**, *10*, 3616.
- [27] J. Chen, J. Yang, Z. L. Li, X. Fan, Y. L. Zi, Q. S. Jing, H. Y. Guo, Z. Wen, K. C. Pradel, S. M. Niu, Z. L. Wang, *ACS Nano* **2015**, *9*, 3324.
- [28] G. Zhu, Y. J. Su, P. Bai, J. Chen, Q. S. Jing, W. Q. Yang, Z. L. Wang, *ACS Nano* **2014**, *8*, 6031.
- [29] Y. J. Su, X. N. Wen, G. Zhu, J. Yang, J. Chen, P. Bai, Z. M. Wu, Y. D. Jiang, Z. L. Wang, *Nano Energy* **2014**, *9*, 186.
- [30] Q. Jing, G. Zhu, P. Bai, Y. Xie, J. Chen, R. P. S. Han, Z. L. Wang, *ACS Nano* **2014**, *8*, 3836.
- [31] J. Chen, J. Yang, H. Guo, Z. Li, L. Zheng, Y. Su, Z. Wen, X. Fan, Z. L. Wang, *ACS Nano* **2015**, *9*, 12334.
- [32] J. Chen, Z. L. Wang, *Joule* **2017**, *1*, 480.
- [33] Z. L. Wang, *Faraday Discuss.* **2014**, *176*, 447.
- [34] Z. L. Wang, *Nature* **2017**, *542*, 159.
- [35] T. Jiang, Y. Y. Yao, L. Xu, L. M. Zhang, T. X. Xiao, Z. L. Wang, *Nano Energy* **2017**, *31*, 560.
- [36] C. Wu, R. Liu, J. Wang, Y. Zi, L. Lin, Z. L. Wang, *Nano Energy* **2017**, *32*, 287.
- [37] Z. Lin, B. Zhang, H. Guo, Z. Wu, H. Zou, J. Yang, Z. L. Wang, *Nano Energy* **2019**, *64*, 103908.
- [38] J. An, Z. Wang, T. Jiang, X. Liang, Z. L. Wang, *Adv. Funct. Mater.* **2019**, *29*, 1904867.